nature communications

Article

https://doi.org/10.1038/s41467-025-62145-7

A SaBOX/Co catalyst designed for facile access to the challenging copolymers of vinyl ester and methacrylate

Received: 20 August 2024

Accepted: 11 July 2025

Published online: 28 July 2025

Check for updates

Yi-Jie Ding[1,2,3], Sheng-Ye Zhang[1,3], Ya-Ning Li[1], Shu-Yang Yu[1], Kongchanghao Huang[1], Yuchen Zhang[1], Jun-Fang Li[1], Xiao-Yan Wang[1] ✉ & Yong Tang[1] ✉

Copolymerization of more activated methacrylates and less activated vinyl esters is challenging because of their large difference in reactivity ratio. This severely limits the development of high-performance materials. Herein, we design a side-armed bisoxazoline (SaBOX)/$CoBr_2$ catalyst with sheltered coordination environment to achieve strong binding ability to propagating radicals in photoinduced cobalt-mediated radical polymerization (CMRP) of vinyl ester and methacrylate. This enables the efficient synthesis and structure regulation of methacrylate-vinyl ester copolymers. The catalytic system efficiently and directly produces di- and tri-block copolymers via in-situ chain extension. Moreover, homogeneous random copolymers of vinyl ester and methacrylate are also facilely synthesized. The mechanistic studies are consistent with the polymerization results, which validate the CMRP mechanism and our catalyst design concept.

It is a great challenge to conveniently synthesize the copolymers of more activated and less activated monomers because of their significant differences in reactivity and polymerization behavior, severely impeding the development of high-performance materials. To overcome this issue, a semi-batch or semi-continuous monomer feeding strategy was developed, in which the monomer with higher activity is slowly added to the system. By this strategy, random and even homogeneous random copolymers of monomers with vastly different reactivity ratios, mostly methyl acrylate (MA) and vinyl acetate (VAc), were successfully synthesized, however, which requires the precise control of feeding process through painstaking design[1–5]. In addition, for two monomers with more immense differences in reactivity, such as methyl methacrylate (MMA) and VAc[6,7], the synthesis of homogeneous random copolymers by this strategy is more challenging and requires more elaborate design and more precise control of the feeding process, otherwise the resulting copolymers would have a very non-uniform composition or even be blends of homopolymers[7–10]. With the excellent design of catalyst or mediator, controlled radical polymerization (CRP) enables the building of precise and complex macromolecular structures[11–16]. However, CRP also fails to efficiently achieve the direct copolymerization of vinyl ester and methacrylate, as almost all CRP systems only can efficiently control the polymerization of one type (more activated or less activated) of vinyl monomer[17–29]. Even the relatively easily accessible di-block copolymers of methacrylate and vinyl ester, were always synthesized by indirect methods, such as the combination of CRP techniques[30–34], the stimuli-responsive RAFT system depending on switching external conditions[17,35] and the post-modification of di-block copolymer of MMA and methyl vinyl ketone[36]. However, all these methods require toilsome synthetic processes and/or exhibit low efficiency, and are difficult to synthesize multi-block and homogeneous random copolymers of vinyl ester and methacrylate. Thus, one strategy for facile access to homogeneous random and block copolymers of vinyl ester and methacrylate has rarely been achieved, let alone the precise regulation of their structures.

To tackle the challenge, we analysed the copolymerization process carefully. As shown in Fig. 1a, during the copolymerization

[1]The State Key Laboratory of Organometallic Chemistry, Shanghai Institute of Organic Chemistry, Chinese Academy of Sciences, Shanghai, China. [2]School of Physical Science and Technology, ShanghaiTech University, Shanghai, China. [3]These authors contributed equally: Yi-Jie Ding, Sheng-Ye Zhang.
✉e-mail: wangxiaoyan@sioc.ac.cn; tangy@sioc.ac.cn

of VAc with MMA, there are 4 different propagation processes. It is thermodynamically unfavourable for the chain end bearing MMA· to attack monomer VAc, due to that the process is the transforming of conjugated 3° carbon radical to non-conjugated 2° carbon radical (usually $\Delta G > 0$) in essence (Fig. 1c) and prone to the reverse reaction. This should be the main obstacle of the copolymerization process. Based on this, we designed a SaBOX/$CoBr_2$ complex as CMRP catalyst, which has tetracoordinated twisted tetrahedral configuration with two side arms towards metal center[37,38]. As the sheltered coordination environment can protect the catalytic centre from coordination of solvents and monomers, compared with the traditional CMRP-catalyst such as cobalt acetylacetonate and porphyrin cobalt[39,40], the SaBOX/$CoBr_2$ catalyst is promising to have stronger binding and stabilizing ability to the propagating radicals, especially those bearing the smaller and more active VAc·. And thus, the thermodynamic stability of the product of MMA· + VAc could be greatly enhanced after being captured by SaBOX/$CoBr_2$ to generate dormant species, inhibiting the reverse reaction and resolving the main obstacle to VAc/MMA copolymerization (Fig. 1d). Considering that the dormant species might be too thermodynamically stable to reactivate, the photo-activation process was introduced to bypass thermodynamic stability and directly activate the dormant species, namely, to promote the cleavage of C-Co in the species to generate radicals for polymerization (Fig. 1e). The SaBOX/$CoBr_2$ catalyst achieves the convenient synthesis of homogeneous random copolymers of vinyl ester and methacrylate with high efficiency and controllability under common photoinduced CMRP conditions[27]. Besides, this catalytic system could directly and efficiently produce the di- and tri-block copolymers of them via in-situ chain extension, without the limitation of monomer feeding order.

Results

CMRP of VAc and ligand effect

We are working on the development of efficient CRP catalytic systems these years and observed strong ligand effects[41–47]. Thus, we first explored the effect of bisoxazoline (BOX)-derived ligands (Fig. 2) in CMRP of VAc, by using in-situ formed BOX/$CoBr_2$ complex as catalyst and TPO as photoinitiator under the irradiation of 24 W white light for 3 h (Table 1). In absence of ligand, the conversion was low (36%) and the polymerization controllability was poor, as the molecular weight was much higher than theoretical value (run 1). When using the isopropyl- or phenyl-substituted BOX ligand (**L1** or **L2**), the polymerization was suppressed (runs 2-3), obtaining even lower conversions. When indane-substituted BOX (In-BOX) **L3** with rigid skeleton was used as ligand, the monomer conversion was comparable with the case without ligand (38%), and the controllability of molecular weight was still poor (run 4). Subsequently, **L4** containing two benzyl side arms was used and faster polymerization rate was obtained, giving 56% conversion in 3 h, but the molecular weight was still much higher than theoretical value (run 5). **L5** containing two pyridine side arms was then employed, as the pyridine side arms might have a remote weak coordination with the metal centre, so as to play a better shielding effect. Despite the molecular structure of **L5**/$CoBr_2$ obtained by X-ray characterization shows that the pyridine side arms do not coordinate with the cobalt centre (Supplementary Fig. 1), they orient towards the metal centre and act as good shelter. As expected, the polymerization by **L5**/$CoBr_2$ was very fast and the polymerization controllability was excellent, giving high conversion of 93% within 3 h with narrowly distributed molecular weight (Đ = 1.23) close to theoretical value (run 6). These results show that both the pyridine arms and the In-BOX skeleton are necessary for an excellent ligand. It should be noted that the polymerization used only 0.1 mL of THF solvent for catalyst preparation and proceeded at a relatively low temperature. Consequently, chain transfer to solvent[48] was not significant, and no obviously reduced molecular weight compared to the theoretical value was observed.

The whole process of VAc polymerization by **L5**/$CoBr_2$ (run 6, Table 1) was tracked and the polymerization kinetics was studied. Analysis reveals first-order kinetics for monomer consumption with negligible induction phase (Fig. 3a). Molecular weights consistently

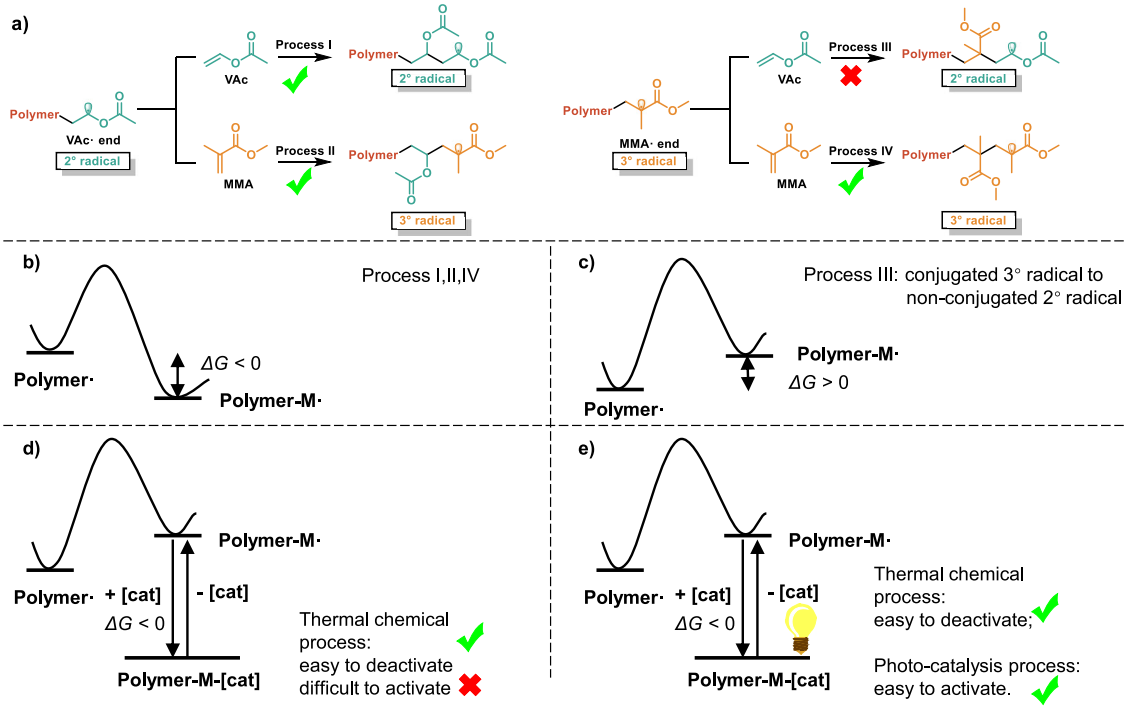

Fig. 1 | The analysis of the VAc/MMA copolymerization process. a Propagation of VAc-terminated chains and MMA-terminated chains. **b** Illustration of energy change in processes I, II, and IV. **c** Illustration of energy change in process III. **d** Illustration of energy change in process III with catalyst. **e** Illustration of energy change in process III with catalyst under sustained photoactivation.

https://doi.org/10.1038/s41467-025-62145-7

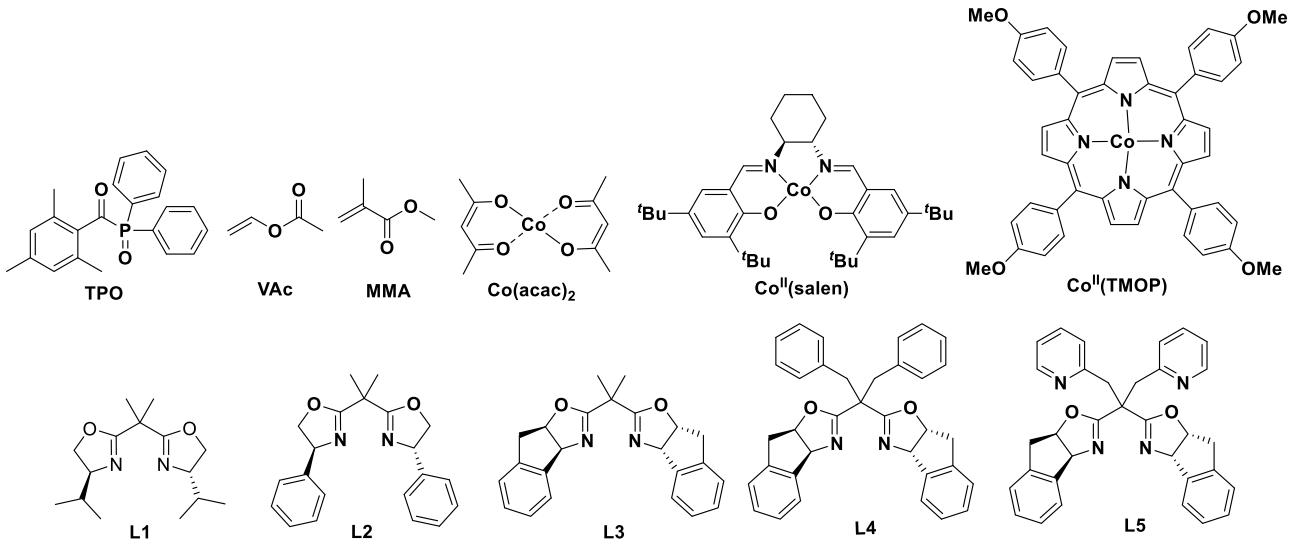

Fig. 2 | The structures of compounds. The structures of ligands, catalysts, initiator, and monomers used in this work.

Table 1 | The photoinduced CMRP using different catalysts

Run[a]	M	DP_{target}	t (h)	Cat.	Conv.[c] (%)	$M_{n,GPC}$ (kg/mol)	Đ	$M_{n,theory}$[d] (kg/mol)
1	VAc	200	3	**$CoBr_2$**	36	20.3	1.45	6.2
2	VAc	200	3	**L1/$CoBr_2$**	18	22.5	1.78	3.1
3	VAc	200	3	**L2/$CoBr_2$**	26	26.7	1.72	4.5
4	VAc	200	3	**L3/$CoBr_2$**	38	26.4	1.52	5.2
5	VAc	200	3	**L4/$CoBr_2$**	56	26.3	1.73	9.6
6	VAc	200	3	**L5/$CoBr_2$**	93	18.6	1.23	16.0
7	MMA	200	9	**L5/$CoBr_2$**	85	21.3	1.35	17.0
8[b]	MMA	200	9	**Co(acac)$_2$**	62	64.6	4.52	12.4
9[b]	MMA	200	9	**Co^{II}(Salen)**	38	36.5	1.79	7.6
10[b]	MMA	200	9	**Co^{II}(TMOP)**	44	30.4	1.67	8.8

[a]4 mmol monomer, using 24 W white light, 0.1 mL THF for VAc, 0.25 mL THF for MMA, at ambient temperature, $[M]_0/[CoBr_2]_0/[Ligand]_0/[TPO]_0 = 200/1/1/0.6$. [b]$[M]_0/[\mathbf{Cat.}]_0/[TPO]_0 = 200/1/0.6$. [c]Determined by ^{1}H NMR. [d]$M_{n,theory} = [Monomer]_0/[Co]_0 \times M_{Monomer} \times Conv$[27].

align with theoretical predictions while maintaining narrow dispersities (Đ = 1.18–1.32) throughout the reaction (Fig. 3b), suggesting characteristics of highly controlled polymerization. In VAc homopolymerization, our **L5**/$CoBr_2$ catalyst achieves molecular weight control matching or surpassing established systems (Co(acac)$_2$, Co^{II}(β-ketiminato), Co^{II}(Salen), etc.[27,49–53]; Fig. 2), as demonstrated by experimental-theoretical value agreement and low dispersity. Excellent temporal regulation and photoswitching capability are shown in Fig. 3c: polymerization immediately initiates upon irradiation ("on" state) and ceases completely in darkness ("off" state) across multiple cycles. The control on molecular weight is preserved under these switching conditions (Fig. 3d). These results indicate that, in the CMRP of VAc, the dormant species generated from the combination of propagating radicals with **L5**/$CoBr_2$ is stable, and the cleavage of C-Co in the species to produce radicals requires the absorption of energy under light (Supplementary Fig. 2), that is, the reactivation of dormant species is controlled by the switching of illumination, so as to facilitate the temporal control of polymerization process. This is one of the advantages of photoinduced CMRP[54] and other forms of photoinduced controlled radical polymerization[44,55–57].

CMRP of MMA

Next, we conducted CMRP of MMA by **L5**/$CoBr_2$. The polymerization was also fast and highly controllable. The monomer conversion was 85% in 9 h, and the molecular weight was close to theoretical value with Đ of 1.35 (run 7). The process was tracked and the polymerization kinetics was studied (Fig. 3e, f), which are consistent with a well-controlled polymerization process. By contrast, in the polymerization of MMA mediated by Co(acac)$_2$, the MMA conversion was 64% in 9 h, but the controllability was very poor (run 8), as the molecular weight was much higher than theoretical value with a very wide Đ of 4.52. Similarly, the catalysts (*S*,*S*)-(+)-*N*,*N*′-Bis(3,5-di-tert-butylsalicylidene)−1,2-cyclohexanediamino cobalt(II) (Co^{II}(Salen)) and cobalt tetramethoxyphenylporphyrin (Co^{II}(TMOP)) also exhibit poor control over the polymerization of MMA, as the resulting polymers have molecular weights significantly higher than the theoretical values and broad molecular weight distributions (runs 9-10). These results are consistent with the literature reports[29] that it is difficult for conventional CMRP catalysts to mediate the controlled polymerization of methacrylates, highlighting the superiority of the **L5**/$CoBr_2$ catalytic system.

The preparation of di-/tri-block copolymers of vinyl esters and methacrylates via in-situ chain extension

As **L5**/$CoBr_2$ catalytic system could efficiently mediate controlled polymerization of both vinyl ester and methacrylate, we attempted to directly synthesize block copolymer of VAc and MMA via in-situ chain extension (Supplementary Table 4). After 4 mmol VAc was nearly completely transformed ($Conv._{VAc}$ = 93%) in 3 h, 4 mmol MMA were

https://doi.org/10.1038/s41467-025-62145-7

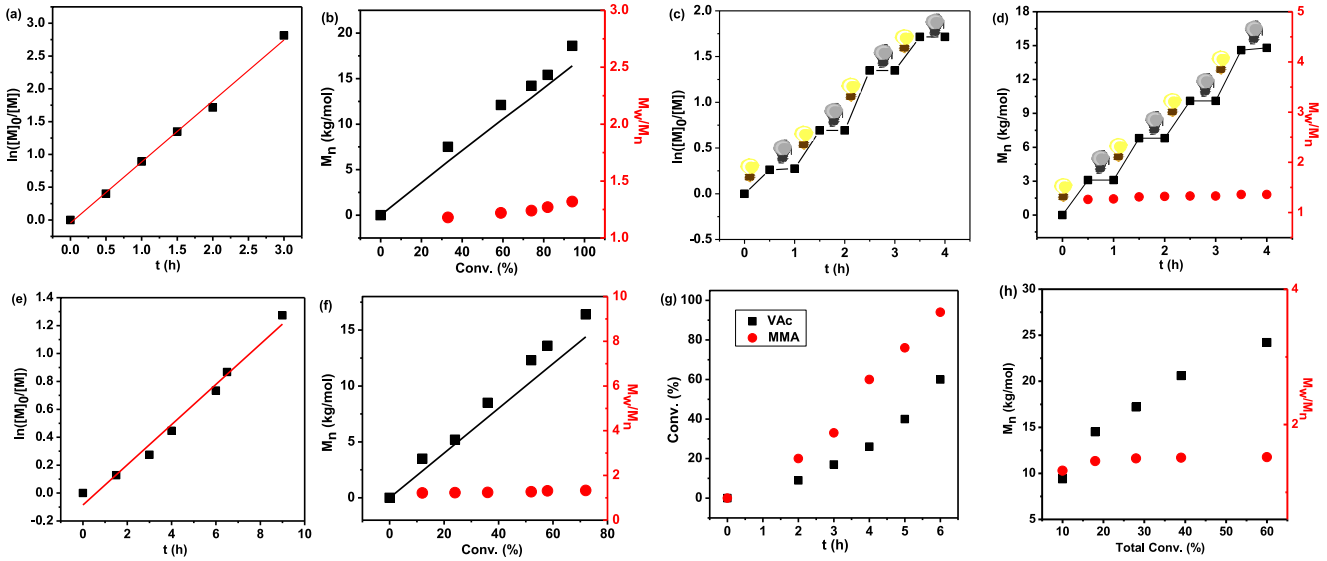

Fig. 3 | Kinetic studies on polymerization. a $\ln([M]_0/[M])$ versus time during the CMRP of VAc (run 6, Table 1). **b** M_n (black) and Đ (M_w/M_n, red) versus conversion during the CMRP of VAc (run 6, Table 1). **c** $\ln([M]_0/[M])$ versus time during the intermittent CMRP of VAc. **d** M_n (black) and Đ (M_w/M_n, red) versus time during the intermittent CMRP of VAc. **e** $\ln([M]_0/[M])$ versus time during the CMRP of MMA (run 7, Table 1). **f** M_n (black) and Đ (M_w/M_n, red) versus conversion during the CMRP of MMA (run 7, Table 1). **g** Monomer conversion versus time during the random VAc/MMA copolymerization with $[VAc]_0/[MMA]_0$ of 10/1 (run 5, Table 2). **h** M_n (black) and Đ (M_w/M_n, red) versus total monomer conversion during the random VAc/MMA copolymerization with $[VAc]_0/[MMA]_0$ of 10/1 (run 5, Table 2).

added. The in-situ chain extension gave MMA conversion of 61% in 6 h. After chain extension, The GPC curve shifted entirely toward the higher molecular weight region, exhibiting a symmetrical peak shape with no tailing (Fig. 4a). The final molecular weight was close to theoretical value with a narrow Đ of 1.35. The kinetics of the chain extension process demonstrates the characteristics of CRP (Supplementary Fig. 3). The isolated block copolymer was thoroughly characterized by a suite of NMR techniques, including ^{1}H NMR, ^{13}C NMR, DEPT 135, two-dimensional NMR analyses (HSQC and HMBC), and DOSY-NMR. The characterization results (Supplementary Figs. 4-9) suggest that the obtained block copolymer PVAc-*b*-PMMA has a structure as designed and expected, with no homopolymer detected. The block copolymer of VAc and MMA was directly prepared via in-situ chain extension in one CRP system, without the combination of different technologies and/or the change of external conditions. By contrast, in the chain extension process mediated by $Co(acac)_2$ under the same conditions, the conversion of MMA was 42% in 6 h, with wide Đ of 1.67 and GPC curve presenting a triple peak (Supplementary Fig. 10), suggesting an obvious residue of the first block. These results verify that the common CMRP catalyst could not prepare the block copolymer of MMA and VAc via in-situ chain extension, further confirming the superiority of our catalytic system. By adding a different methacrylate as second monomer, the block copolymer of VAc and 2-methoxyethyl methacrylate (MEMA) was also successfully synthesized (Fig. 4b). Similarly, the block copolymers of vinyl pivalate (VPi) and MMA was conveniently produced by adding VPi as the first monomer (Fig. 4c).

Besides, we changed the monomer feeding order and successfully synthesized di-block copolymer PMMA-*b*-PVAc, with MMA and VAc conversions of 99% and 64%, respectively. The final molecular weight is close to theoretical value, and the GPC peak is symmetrical (Fig. 4d) with a relatively narrow distribution (Đ = 1.46). The MALDI-TOF MS spectrum of low-molecular-weight PMMA-*b*-PVAc, synthesized at low targeted polymerization degree and purified via quenching-adsorption steps to remove C-Co end groups (Supplementary Fig. 16), supports the formation of a block copolymer, as a single polymer chain contains both VAc and MMA units. The peak pattern exhibits discrete characteristics, with signal peaks corresponding to combinations of different block lengths[58,59]. This result demonstrates that **L5**/$CoBr_2$ mediated the synthesis of block copolymers of vinyl ester and methacrylate is not limited by monomer feeding order. Based on this, we conveniently synthesized the tri-block copolymers of vinyl ester and methacrylate via in-situ chain extension, in which the three monomers VAc, MMA and vinyl butyrate (VBu) were added successively (Supplementary Table 6). After each chain extension, the GPC curve moved towards higher molecular weight with a final Đ of 1.40, and the GPC peak patterns were symmetrical without any tailing or shoulder peak (Fig. 4e). The triblock copolymer PMMA-*b*-PVAc-*b*-PMEMA was also facilely synthesized by changing the feeding sequence of vinyl ester and methacrylate (Fig. 4f). Triblock copolymers between various vinyl esters and methacrylates can be produced in any order by a single catalyst. These results further demonstrate that **L5**/$CoBr_2$ is the long-awaited and excellent CRP catalytic system that is really adapt to both vinyl esters and methacrylates.

Random copolymerization of VAc with MMA

In absence of catalyst, ignorable VAc conversion (<5%) was detected when MMA conversion reached 95% (Table 2, run 1) in the random VAc/MMA copolymerization ($[MMA]_0/[VAc]_0 = 1/10$). This result is consistent with literature reports[6,7]. The same result was obtained when introducing $Co(acac)_2$, Co^{II}(Salen) or Co^{II} (TMOP) as CMRP catalyst (Table 2, runs 2-4), demonstrating that common CMRP catalysts also could not mediate the homogeneous random VAc/MMA copolymerization.

As the synthesis of block copolymers of vinyl ester and methacrylate by **L5**/$CoBr_2$ is not limited by monomer feeding order, which indicates that this catalytic system could achieve interlaced chain propagation of vinyl ester and methacrylate, and thus is promising to efficiently regulate random VAc/MMA copolymerization. We conducted the random VAc/MMA copolymerization using **L5**/$CoBr_2$ as catalyst, by setting $[MMA]_0/[VAc]_0$ as 1/10 and 1/20, respectively (Table 2, runs 5 - 6). The reactions were stopped after 6 h and 2.5 h, respectively, yielding VAc/MMA conversions of 54%/94% and 55%/93%. The molar ratios of VAc and MMA units in the isolated copolymers are 6.4/1 and 12.0/1, respectively, close to the values calculated based on the feeding ratio and conversions of VAc and MMA ([VAc unit]/[MMA

https://doi.org/10.1038/s41467-025-62145-7

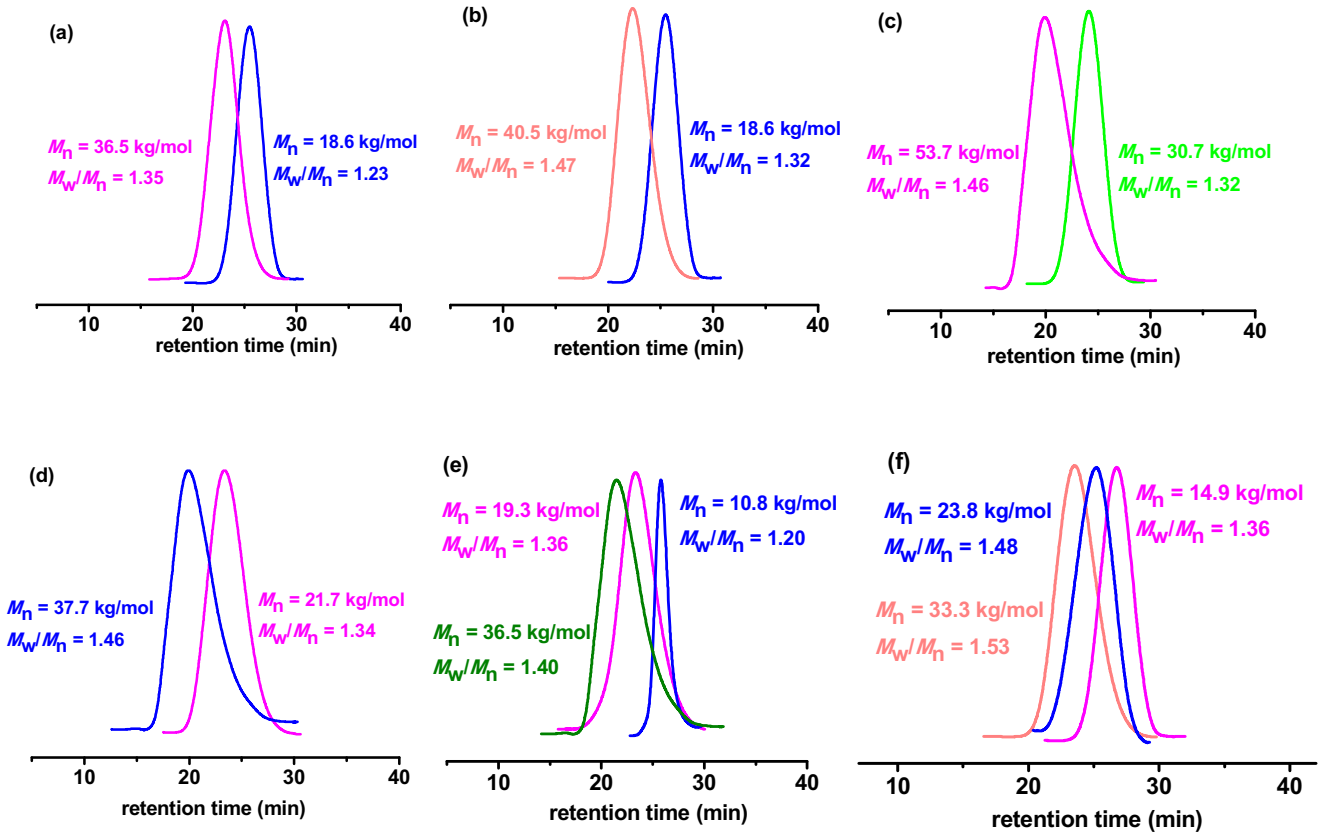

Fig. 4 | The GPC traces of the synthesis of block copolymers via in-situ chain extension by L5/$CoBr_2$. **a** PVAc (blue line) and PVAc-*b*-PMMA (pink line). **b** PVAc (blue line) and PVAc-*b*-PMEMA (pale pink line). **c** PVPi (green line) and PVPi-*b*-PMMA (pink line). **d** PMMA (pink line) and PMMA-*b*-PVAc (blue line). **e** PVAc (blue line), PVAc-*b*-PMMA (pink line) and PVAc-*b*-PMMA-*b*-PVBu (dark green line). **f** PMMA (pink line), PMMA-*b*-PVAc (blue line) and PMMA-*b*-PVAc-*b*-PMEMA (pale pink line).

unit]$_{calculation}$). The GPC curves show single distribution, with Đ of 1.4 ~ 1.5. The random copolymerization of VAc and MMA involves two radicals and two monomers with large differences in reactivity, leading to substantial differences in the rates of the four chain propagation reactions. Additionally, the reaction also involves the formation and reactivation of two types of dormant species. These factors collectively exacerbate the heterogeneity in polymer chain size. Therefore, the control over the molecular weight in the random VAc/MMA copolymerizations is inferior, compared with the cases of VAc or MMA homopolymerizations. We tracked the copolymerization process with $[VAc]_0/[MMA]_0$ of 10/1 (Supplementary Table 7). In the whole copolymerization process (Fig. 3g), MMA was converted faster than VAc, but both monomers were gradually consumed with time. The conversion ratio of two monomers varied in a small range (1.7 ~ 2.4) during the whole random copolymerization of MMA and VAc, indicating that the MMA/VAc copolymer synthesized by **L5**/$CoBr_2$ has a relatively uniform composition. Besides, the molecular weights gradually increased over the total monomer conversion and with relatively narrow Đs of 1.3 ~ 1.5 (Fig. 3h), meaning a sufficiently high frequency of activation-deactivation cycle and suggesting the characterizations of "living" radical polymerization. Comprehensive NMR characterization (^{1}H NMR, ^{13}C NMR, DEPT 135, HSQC and HMBC) of the resultant copolymer (Supplementary Figs. 11-15) reveals that the carbon signals of -CH_2- in the polymer backbone were not concentrated at 39 ppm, caused by the continuous insertion of VAc, and at 54 ppm, caused by the continuous insertion of MMA, respectively. Instead, the signals were dispersed between 39 and 54 ppm, indicating that the MMA and VAc units are randomly distributed along the polymer chain. The MALDI-TOF MS spectrum of low-molecular-weight poly(MMA-*co*-VAc), synthesized at low targeted polymerization degree and purified by quenching and adsorption to remove C-Co end groups (Supplementary Fig. 16), supports the formation of a homogeneous random copolymer, with a single polymer chain containing both VAc and MMA units. Due to the random monomer arrangement, its peak pattern shows a continuous distribution, where the mass differences between adjacent peaks primarily correspond to the mass differences of the monomer units[58,60]. The DOSY-NMR spectrum shows only one diffusion coefficient for the polymer (Supplementary Fig. 17), confirming that the random copolymer has a relatively uniform structure and the content of homopolymers can be ignored. According to the literatures[2,3,5,6,21,61,62], the resultant MMA/VAc copolymer with a relatively uniform structure can be called homogeneous random copolymer.

Although the focus of this study is on the copolymerizations of vinyl esters with methacrylates, we have also employed **L5**/$CoBr_2$ catalyst to conduct the random copolymerization of VAc with another type of more activated monomer, N,N-dimethylacrylamide (DMA), under similar conditions, by setting $[DMA]_0/[VAc]_0$ as 1/10 (Supplementary Table 8). The DOSY-NMR spectrum shows only one diffusion coefficient (Supplementary Fig. 18) for the polymer, confirming that the resultant random copolymer has a relatively uniform structure and the content of homopolymers can be ignored. We also directly synthesize the block copolymer of VAc and DMA via in-situ chain extension (Supplementary Table 4). After chain extension, GPC curve moved towards higher molecular weight with a symmetrical peak pattern (Supplementary Fig. 19). The final molecular weight was close to the theoretical value with a relatively narrow Đ of 1.38. These results indicate that our catalytic system has the potential to efficiently access challenging copolymers of other two kinds of monomers with large difference in reactivity.

Table 2 | The random copolymerization of VAc with MMA

Run	Cat.	$[VAc]_0/[MMA]_0$	t (h)	Conv. (%)[d] (VAc/MMA)	$M_{n,GPC}$ (kg/mol)	Đ	[VAc unit]/ [MMA unit]	$([VAc\ unit]/[MMA\ unit])_{calculation}$[e]
1[a]	/	10/1	14	trace/95	/	/	/	/
2[b]	**$Co(acac)_2$**	10/1	14	trace/92	/	/	/	/
3[b]	**Co^{II}(Salen)**	10/1	14	trace/94	/	/	/	/
4[b]	**Co^{II}(TMP)**	10/1	14	trace/>99	/	/	/	/
5[c]	**L5/$CoBr_2$**	10/1	6	54/94	24.2	1.52	6.4/1	5.7/1
6[c]	**L5/$CoBr_2$**	20/1	2.5	55/93	26.5	1.42	12.0/1	11.8/1

Reaction condition: using 24 W white light at ambient temperature, 4 mmol VAc, 0.1 mL THF. [a]$[VAc]_0/[TPO]_0 = 200/0.6$. [b]$[VAc]_0/[\mathbf{Cat.}]_0/[TPO]_0 = 200/1/0.6$. [c]$[VAc]_0/[CoBr_2]_0/[\mathbf{L5}]_0/[TPO]_0 = 200/1/1/0.6$. [d]Determined by ^{1}H NMR. [e]Calculated based on the feeding ratio and conversions of VAc and MMA.

The thermodynamic properties of the typical copolymers

The glass transition temperatures (T_g) of the homopolymers PVAc and PMMA (Table 1, runs 1 and 7) were 42 °C and 129 °C, respectively (Supplementary Fig. 20 and Supplementary Table 9). The T_gs observed for PVAc and PMMA in this study are higher than the typically reported values[63]. We speculate that the enhanced chain regularity of polymers obtained via controlled radical polymerization at ambient temperature, compared to those produced by conventional radical polymerization at elevated temperatures, may account for this T_g elevation. The initial degradation temperature of PMMA is significantly lower than that of PVAc ($T_{d,5}$ = 261 °C versus 316 °C) (Supplementary Fig. 21). Besides, the degradation of PMMA occurs rapidly in a single stage, corresponding to the scission of the main chain, whereas the degradation of PVAc occurs in two distinct stages, involving initial side-group elimination followed by backbone decomposition. PVAc and PMMA end their degradation at 550 °C and 410 °C, respectively. By comparison, PVAc exhibits higher thermal stability than PMMA. For random copolymer poly(MMA-*co*-VAc) with a VAc and MMA unit ratio of 6.4/1 (Table 2, run 5), the T_g is 48 °C, and degradation also occurs in two stages. But both the initiation and termination of the second-stage thermal degradation occur earlier than those of PVAc. These results suggest that the random introduction of relatively rigid MMA units into the chain of PVAc increases T_g, and promotes thermal degradation, aligning with the highly reversible cross-propagation process present in the VAc/MMA copolymerization. For the block copolymer PVAc-*b*-PMMA (Supplementary Table 4, run 2), the thermodynamic property lies between those of homopolymers PVAc and PMMA. There are two T_gs, at 45 °C and 126 °C, respectively. The degradation occurs in two stages, starting at 315 °C and ending at 520 °C.

Mechanism studies

CMRP or ATRP. Since the **L5**/$CoBr_2$ complex bears bromine, it is assumed that the polymerization might follow ATRP mechanism. Therefore, it is important to find out the polymerization mechanism. First, we conducted the DFT calculations towards CMRP deactivation (process A). For simplification, VAc· and MMA· were used to represent propagating chains bearing VAc· and MMA·, respectively. As shown in Fig. 5a, the CMRP deactivation process is favorable thermodynamically according to the binding energy of **L5**/$CoBr_2$ towards VAc· ($\Delta G_{VAc\cdot}^{A} = -14.5$ kcal/mol, $\Delta H_{VAc\cdot}^{A} = -33.3$ kcal/mol) and MMA· ($\Delta G_{MMA\cdot}^{A} = -3.8$ kcal/mol, $\Delta H_{MMA\cdot}^{A} = -12.9$ kcal/mol). Therefore, **L5**/$CoBr_2$ can act as an efficient CMRP deactivator for polymerizations of both VAc and MMA to maintain low radical concentration and avoid side reactions, and thus achieve excellent polymerization controllability. We also conducted DFT calculations towards ATRP deactivation (process E, Supplementary Note 2). For polymerizations of both VAc and MMA, the ATRP deactivation is a process of absorbing energy (6.7 kcal/mol and 17.1 kcal/mol, respectively), which is very unfavorable in thermodynamics. Therefore, ATRP mechanism looks unworkable for the polymerizations of MMA and VAc by **L5**/$CoBr_2$.

In order to further verify the CMRP mechanism, we found out whether the end of the "living" polymer chain contains C-Br or C-Co bond by carrying out the cobalt-mediated radical coupling (CMRC) reaction towards PVAc obtained under the same conditions as run 6 in Table 1. When the conversion reached 94%, isoprene was added in situ as coupling reagent ($[VAc]_0/[IP]_0/[CoBr_2]_0 = 200/37/1$). After 2 h, the molecular weight of the polymer doubled to 40.4 kg/mol, which suggests that the polymer end contains C-Co bond (run 1, Supplementary Table 10). Compared with VAc polymerization, MMA polymerization seems to be more likely to follow ATRP mechanism, as the well-controlled CMRP of MMA is very difficult to realize. Therefore, we also conducted the CMRC reaction of PMMA (M_n = 22.2 kg/mol) obtained under the same conditions as run 7 in Table 1 (run 2, Supplementary Table 10), which also resulted in the doubling of molecular weight (M_n = 45.8 kg/mol). This result suggests that the chain of the resultant PMMA (run 7, Table 1) bears C-Co end. On the contrary, the doubling of molecular weight was not detected after the atom transfer radical coupling (ATRC) reaction (n(Cu)/n(Ligand)/n($CuBr_2$)/n(PMMA1)/n(styrene) = 16/8/4/1/2) of low molecular weight PMMA (PMMA1, M_n = 6.4 kg/mol), which was prepared with a low monomer conversion of 42% under the CMRP conditions as run 7 in Table 1 and sufficiently purified by removal of metal complex (run 3, Supplementary Table 10). This result demonstrates that PMMA1 does not contain C-Br end.

Under the similar conditions as Table 1 and Table 2, respectively, low molecular weight PVAc and PMMA were synthesized at low conversion without removal of metal. Notably, the laser irradiation in MALDI-TOF MS measurement readily causes cleavage of the fragile C-Co chain end. After cleavage, chain transfer to solvent, impurities, etc., leads to the formation of polymers containing H at the chain end. Consequently, detecting PVAc chains with C-Co chain ends via MALDI-TOF MS is challenging[27], even though the C-Co bond at the PVAc chain ends is relatively stable. Based on the significant difference in binding energy of the catalyst towards MMA· and VAc· radicals ($\Delta G_{VAc\cdot}^{A} = -14.5$ kcal/mol vs. $\Delta G_{MMA\cdot}^{A} = -3.8$ kcal/mol), the C-Co bond at the PMMA chain end is particularly fragile, making the detection of cobalt-terminated PMMA signals more difficult. The MALDI-TOF MS measurements of both PVAc and PMMA successfully detected peaks corresponding to cobalt-terminated chains (Supplementary Fig. 16), although the signals for PMMA-Co were very weak due to the high fragility of C-Co bond. In the MALDI-TOF MS spectra, no C-Br terminated polymer components were observed. After rigorous purification to remove metal complexes, no bromine was detected (<0.01 wt%) by elemental analysis for both low molecular weight PVAc and PMMA.

The results of these characterizations and control experiments are consistent with the DFT calculations. Together, they demonstrate that the homopolymers of vinyl ester and methacrylate obtained by **L5**/$CoBr_2$ contain C-Co rather than C-Br at the chain end and the CRP in this work follows CMRP rather than ATRP mechanism. In the CMRP process, TPO is cleaved under irradiation, and the generated radicals initiate the continuous addition with monomers to form propagating

https://doi.org/10.1038/s41467-025-62145-7

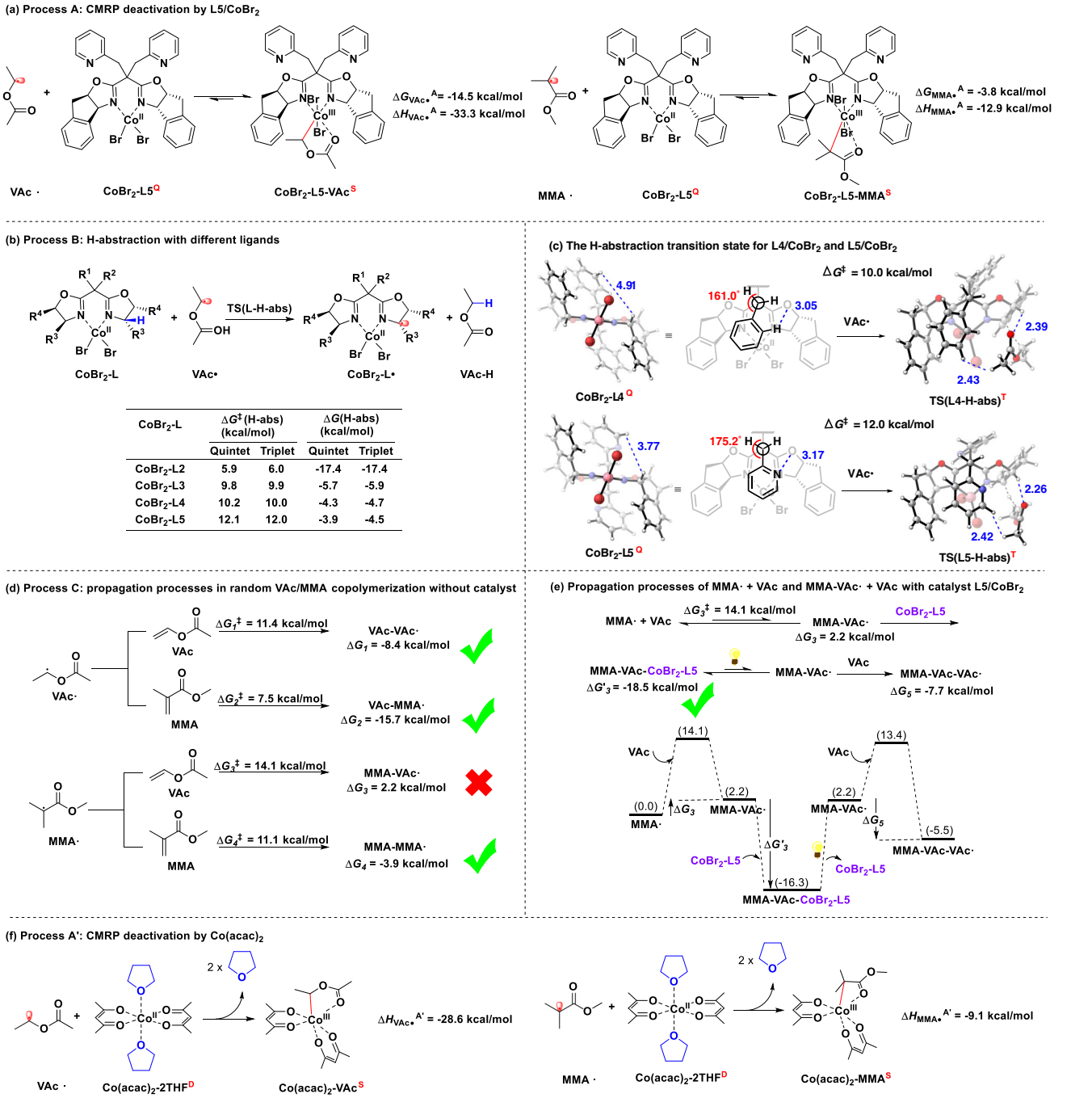

$CoBr_2$-L	ΔG‡(H-abs) (kcal/mol)		ΔG(H-abs) (kcal/mol)	
	Quintet	Triplet	Quintet	Triplet
$CoBr_2$-L2	5.9	6.0	-17.4	-17.4
$CoBr_2$-L3	9.8	9.9	-5.7	-5.9
$CoBr_2$-L4	10.2	10.0	-4.3	-4.7
$CoBr_2$-L5	12.1	12.0	-3.9	-4.5

Fig. 5 | DFT calculations. a Process A: CMRP deactivation by **L5**/$CoBr_2$. **b** Process B: H-abstraction with different ligands. **c** The H-abstraction transition state for **L4**/$CoBr_2$ and **L5**/$CoBr_2$. **d** Process C: propagation processes in random VAc/MMA copolymerization without catalyst. **e** Propagation processes of MMA· + VAc and MMA-VAc· + VAc with catalyst **L5**/$CoBr_2$. **f** Process A': CMRP deactivation by $Co(acac)_2$.

radicals, which are reversibly deactivated by cobalt complex (Supplementary Fig. 2)[21].

Ligand effects. The polymerization results indicate significant ligand effects, that is, both the pyridine arms and the indane-substituted BOX skeleton of the ligand are necessary for an efficient and controlled polymerization. We also performed DFT calculations on the CMRP deactivation process regulated by other four BOX/$CoBr_2$ catalysts (**L1**/$CoBr_2$ to **L4**/$CoBr_2$), that is, the DFT calculations on the binding ability of these catalysts towards propagating radicals. The results show that the four catalysts are very efficient in binding propagating radicals, in other words, the CMRP deactivation processes regulated by **L1**/$CoBr_2$ to **L4**/$CoBr_2$ are favorable thermodynamically (Supplementary Fig. 26). In the CMRC reaction using isoprene as coupling agent, the molecular weight of the PVAc obtained by **L4**/$CoBr_2$ increased significantly (Supplementary Table 10, run 5), indicating that some of the polymers were coupled and these polymers contained C-Co bonds at the chain end, that is, there is a binding interaction between the catalyst and propagating radicals. These results suggest that for the series of BOX/$CoBr_2$ catalysts, the binding strength towards propagating radicals is not the determining factor in controlling the polymerization.

It was found that the VAc polymerization using phenyl-substituted BOX ligand (**L2**) is suppressed, compared with the case in the absence of ligand (Table 1), which indicates that **L2** in the cobalt complex might

quench the propagating radical. The DFT calculation finds out that the tertiary H of BOX might be abstracted by VAc· (Fig. 5b, process B). Although the spin state of the transition state **TS(L-H-abs)** and the corresponding side-product **$CoBr_2$-L·** can be quintet or triplet, the calculation results showed that the influence of the spin state on energy is quite small. For the complex with **L2**, this H-abstraction process is much more favorable than the chain propagation process (VAc· + VAc in process C, Fig. 5d) both dynamically and thermodynamically, with energy barriers ($\Delta G^{\ddagger}$) of 5.9 kcal/mol versus 11.4 kcal/mol and releasing energy (ΔG) of −17.4 kcal/mol versus −8.4 kcal/mol. That is, the radical quenching reaction is irreversible once occurs. This process leads to the destruction of the ligand structure and results in significant chain termination from the early stages of polymerization. As a result, the catalyst **L2**/$CoBr_2$ exhibits poor control over the polymerization, obtaining polymers with higher molecular weight than predicted and broad molecular weight distribution. The calculation shows that the energy barrier and heat release of the H-abstraction process are similar to those of the chain propagation process by the catalyst with rigid In-BOX **L3**, suggesting that these two processes are competitive and radical quenching is unavoidable. By contrast, for the catalyst with ligand containing two pyridine arms (**L5**), the H-abstraction process is dynamically and thermodynamically unfavorable, compared with the chain propagation process (VAc· + VAc in process C). This suggests that two pyridine arms can effectively prevent the propagating radicals from grabbing the H on BOX, thus protecting the polymer chain from being terminated and resulting in well-controlled polymerization. The molecular structure of **L5**/$CoBr_2$ obtained by X-ray characterization shows that the pyridine side arms do not coordinate with the cobalt center (Supplementary Fig. 1). However, the presence of pyridine arms leads to a sheltered conformation of the complex with large steric hindrance. That is, the pyridine side arms enfold the metal center and the active H on BOX. It is conceivable that **L3** without side arms is unable to well protect the metal center and the corresponding active H.

In terms of the H-abstraction reaction, the case for the system of **L4** with benzyl side arms is between those for the **L3** and **L5** systems, in both dynamic and thermodynamic. Notably, the results of the competitive reactions (the propagation reaction and the H-abstraction reaction) depend on the relative activation free energy between them. The activation free energy $\Delta G^{\ddagger}$ of the VAc polymerization is 11.4 kcal/mol, while the $\Delta G^{\ddagger}$ for VAc· radical to abstract the H atom of the ligands **L1** to **L4** and **L5** is 5.9 ~ 10.2 kcal/mol and 12.1 kcal/mol, respectively. Therefore, among all the BOX/$CoBr_2$ catalysts we studied, only for **L5**/$CoBr_2$, the H-abstraction reaction would be well suppressed as its $\Delta G^{\ddagger}$ is higher than that of the polymerization reaction. For the ligands **L4** and **L5** with similar structures, the difference in the $\Delta G^{\ddagger}$ for the H-abstraction reaction is small (1.9 kcal/mol). However, according to Boltzmann distribution, at 298.15 K, the 1.9 kcal/mol $\Delta\Delta G^{\ddagger}$ between **L4** and **L5** is equal to 25 times reaction rate. Besides, as indicated by the shortest distance between the side arm and the active H (4.91 Å versus 3.77 Å, Fig. 5c), compared with the pyridine side arms, the phenyl side arms deviate away from the oxazoline skeleton and expose more space for H-abstraction. This might be due to that the hindrance of C-H in phenyl is larger than the N atom of pyridine. Thus, the phenyl side arm in **L4** would be pushed farther away from the center by the O atom of the skeleton compared with the pyridine side arm in **L5** (161.0° versus 176.2°). Due to the different conformation of the side arm, in the H-abstraction transition state (**TS(L4-H-abs)^T** and **TS(L5-H-abs)^T**), the shorter distance between the skeleton and VAc· is shown in **TS(L5-H-abs)^T** (2.26 Å for **L5** and 2.39 Å for **L4**), which indicates larger steric repulsion and thermodynamic instability for **TS(L5-H-abs)^T** ($\Delta G^{\ddagger}$ = 12.0 kcal/mol (**L5**) versus 10.0 kcal/mol (**L4**)). Thus, the pyridine side arms can better suppress the H-abstraction process.

For the above mechanism studies, we carried out control experiments. Under conditions similar to Table 1, VAc polymerization was carried out using **L3** and **L5** as ligands, respectively, and the polymerization was stopped after 30 min. The retention degree of the corresponding active H on BOX skeleton (Fig. 5b) was detected as 88% and 98% for the systems with **L3** and **L5**, respectively. For the system with **L2**, even if the polymerization was stopped within 10 min, the retention degree of the corresponding active H was only 38%. These results are consistent with the DFT calculations above, which indicate that both In-BOX skeleton and pyridine side arms inhibit the H-abstraction process (radical termination side reaction), thus they are necessary for an efficient and controlled polymerization.

The random VAc/MMA copolymerization. As well recognized in the literatures including textbooks[64,65], many radical chain propagation processes are reversible, probably due to that some products of radical addition reactions are very thermodynamically unstable. We conducted the DFT calculations of different kinds of chain propagation processes in random VAc/MMA copolymerization. In absence of catalyst, it is more favorable for propagating chain to attack the more activated monomer MMA than VAc, both kinetically and thermodynamically, whether the chain end bears MMA· or VAc· (Process C, Fig. 5d). Three of the four chain propagation reactions are thermodynamically favorable and can proceed readily without the need for a catalyst to alter the reaction tendency. Crucially, as we hypothesized, the process for MMA· + VAc is nearly impossible to proceed or thermodynamically inhibited (ΔG_3 = 2.2 kcal/mol), because it involves the transformation from a tertiary radical to a secondary radical, which should be the fundamental obstacle of random VAc/MMA copolymerization. Once the radical MMA· forms, the whole system tends to the self-propagation of MMA. Therefore, in the radical copolymerization system, MMA is first converted to near depletion before VAc polymerization begins, producing blends of homopolymers, and homogeneous random VAc/MMA copolymerization cannot be realized. **L5**/$CoBr_2$ exhibits a very strong binding affinity for the VAc· chain end ($\Delta G_{VAc\cdot}^{A}$ = −14.5 kcal/mol, Process A, Fig. 5a), and the complexation reaction between the propagating radical MMA-VAc· and the catalyst is highly thermodynamically favorable ($\Delta G'_3$ = −18.5 kcal/mol, Fig. 5e). Therefore, the product of this propagation reaction can be stabilized, preventing the reverse reaction, which makes it possible for propagating chains with MMA· to efficiently attack monomer VAc.

In the absence of catalyst **L5**/$CoBr_2$, the nascent MMA-VAc· propagating radical faces two pathways: chain propagation (MMA-VAc· + VAc → MMA-VAc-VAc·) or depropagation (MMA-VAc· → MMA· + VAc). The activation energies for these two paths are very close (11.2 kcal/mol vs. 11.9 kcal/mol, respectively), suggesting they should be in intense competition. However, depropagation holds a kinetic advantage as it is a diffusion-independent unimolecular process, whereas propagation is a bimolecular reaction constrained by diffusion. Consequently, without the catalyst, depropagation predominates and occurs readily, severely impeding MMA/VAc copolymerization. The critical function of **L5**/$CoBr_2$ lies in its effective suppression of this detrimental depropagation pathway, enabled by the catalyst's strong complexation affinity for the MMA-VAc· radical. Under sustained photoactivation, **L5**/$CoBr_2$ mediates barrierless, rapid, and reversible radical capture, forming a stable intermediate ($\Delta G'_3$ = −18.5 kacl/mol, Fig. 5e). This sequestration efficiently suppresses the depropagation reaction, which possesses a significant inherent barrier (11.9 kcal/mol). The deactivation/activation cycle persists until the transiently released propagating radical randomly collides with and attacks a proximal VAc monomer. This propagation step is thermodynamically favored (ΔG_5 = −7.7 kcal/mol, Fig. 5e), yielding the stable MMA-VAc-VAc· adduct. Thus, through strong complexation, **L5**/$CoBr_2$ significantly eliminates the "completely free" MMA-VAc· radical that is prone to depropagation. This propagating radical exists predominantly either catalyst-bound or actively propagating. The suppression of the

depropagation pathway of MMA-VAc· radical by catalyst **L5**/$CoBr_2$ facilitates efficient VAc/MMA copolymerization.

In addition, DFT calculations suggest that the catalyst exerts no acceleration effect on the propagation processes since it does not participate in their kinetics (Supplementary Note 4). The propagation and the deactivation of its product are stepwise processes. Consequently, the critical role of catalyst **L5**/$CoBr_2$ in the random copolymerization of MMA and VAc lies in affecting the thermodynamics of the key propagation process, namely, the catalyst can efficiently bind the addition product of propagating chains bearing MMA· with VAc to prevent the reverse reaction.

The reactivity ratios of MMA and VAc were determined by low conversion copolymer composition experiments. The average reactivity ratios are calculated as r(MMA) = 7.850 and r(VAc) = 0.698, respectively, via Fineman-Ross, Mayo-Lewis and Kelen-Tudos methods (Supplementary Table 11, Supplementary Fig. 22)[66,67]. As reported[6,7], the reactivity ratios of MMA and VAc in free radical copolymerization differ by more than three orders of magnitude, for example, r(MMA) = 27.8 and r(VAc) = 0.014. Therefore, the difference of reactivity between MMA and VAc is significantly reduced by the **L5**/$CoBr_2$ catalytic system. Notably, it is meaningless to compare the specific values of reactivity ratio here, because the methods used to calculate reactivity ratio in the literature do not consider that the chain propagation might be reversible, that is, the premise of these methods is that each step of chain propagation is irreversible. As mentioned above, it is believed that the main obstacle of the random MMA/VAc copolymerization is that the product of MMA· + VAc is thermodynamically unstable. This step of cross-propagation is highly reversible or thermodynamically inhibited (ΔG = 2.2 kcal/mol). Therefore, the premise of the methods used in the previous literature to calculate the reactivity ratios of MMA and VAc might not be valid[7,68,69]. Therefore, we also fitted the kinetic data of VAc/MMA copolymerization ([VAc]/[MMA] = 10/1) to the Beckingham–Sanoja–Lynd (BSL) copolymerization model to determine reactivity ratios (Supplementary Note 5)[55]. This method does not require changing the monomer composition, and the reactivity ratios are calculated based on the kinetics of one copolymerization reaction. The values of reactivity ratio were determined as r(MMA) = 3.133 and r(VAc) = 0.316 using BSL integrated model. Besides, we also employed the method recommended by IUPAC[70] to determine the reactivity ratios from copolymer composition and overall conversion measurements, by carrying out four reactions at three different initial feeding compositions. The IUPAC method was implemented in the existing free ware Contour (Supplementary Table 12), giving the values of reactivity ratio as r(MMA) = 4.052 and r(VAc) = 0.435, which are on the same order of magnitude as those obtained by the classical linear methods and BSL method.

The above reactivity ratio data indicate that although catalyst **L5**/$CoBr_2$ can promote the effective VAc/MMA copolymerization, the reactivity ratio of MMA remains significantly higher than that of VAc (differing by approximately an order of magnitude) in the random copolymerization by **L5**/$CoBr_2$. Consequently, a relatively high concentration of VAc relative to MMA (e.g., 10/1) is required for the copolymerization to proceed effectively.

Comparison with one typical CMRP catalyst. At last, we would like to illustrate the superiority of **L5**/$CoBr_2$ to one typical CMRP-catalyst, $Co(acac)_2$. According to literatures, $Co(acac)_2$ is complexed with THF in THF solution[31]. Since it is difficult to consider the chemical potential of solvent THF, the enthalpy change (ΔH) is used to estimate the binding ability of $Co(acac)_2$ to propagating radicals (Process A′, Fig. 5f). In terms of ΔH, $Co(acac)_2$ is obviously worse than **L5**/$CoBr_2$ for binding propagating chains, whether the chain end bears MMA· or VAc·. ($\Delta H_{VAc\cdot}^{A}$ = −33.3 kcal/mol (**L5**/$CoBr_2$) versus $\Delta H_{VAc\cdot}^{A'}$ = −28.6 kcal/mol ($Co(acac)_2$), $\Delta H_{MMA\cdot}^{A}$ = −12.9 kcal/mol (**L5**/$CoBr_2$) versus $\Delta H_{MMA\cdot}^{A'}$ = −9.1 kcal/mol ($Co(acac)_2$)). As reported, CMRP of VAc mediated by $Co(acac)_2$ could proceed smoothly at 30 °C without irradiation[27], while VAc polymerization could not proceed by **L5**/$CoBr_2$ when the light was turned off, which show that the ability of $Co(acac)_2$ to bind propagating chain is indeed much worse than that of **L5**/$CoBr_2$. Therefore, thanks to the strong enough ability to bind or trap propagating chains, which leads to the efficient deactivation process and levelling effect on the reactivity of monomers, **L5**/$CoBr_2$ can not only well regulate the homopolymerizations of methacrylates and vinyl esters, but also conveniently achieve the challenging homogeneous random copolymerization and block copolymerization of these two kinds of monomers with high efficiency.

On the other hand, we conducted kinetic studies on the $Co(acac)_2$-mediated polymerization of MMA and found that there is an induction period during this process (run 7, Table 1). After this induction period, the polymerization rate by $Co(acac)_2$ is faster than that of the **L5**/$CoBr_2$ system (Supplementary Fig. 30). According to literature[53], the induction period in the $Co(acac)_2$ system is attributed to the need for radicals to react with the cobalt(II) complex, in situ generating a dormant species (cobalt(III) complex), which serves as a clean source of radicals for polymerization. However, the real cause of the induction period remains uncertain and lacks definitive evidence. In our catalytic system, no obvious induction period was observed in both CMRP of MMA and VAc. This might be because, compared to $Co(acac)_2$, while the **L5**/$CoBr_2$ catalyst has a stronger binding ability to the propagating radicals, it has a weaker binding ability to the initial radicals generated from the cleavage of initiators (Processes F and F′). Therefore, in the **L5**/$CoBr_2$ catalytic system, not only the deactivation process can efficiently occur, avoiding the occurrence of side reactions, but also the formation and reactivation of dormant species can efficiently and reversibly proceed at the early stage, resulting in no obvious induction period. The DFT calculations (Supplementary Fig. 31) on the binding energies of both catalysts with the initial radicals support the above hypothesis (ΔH_1^{F} = −37.3 kcal/mol (**L5**/$CoBr_2$) versus $\Delta H_1^{F'}$ = −46.7 kcal/mol ($Co(acac)_2$), ΔH_2^{F} = −31.5 kcal/mol (**L5**/$CoBr_2$) versus $\Delta H_2^{F'}$ = −41.0 kcal/mol ($Co(acac)_2$)).

Discussion

We have developed a SaBOX/$CoBr_2$ catalyst for photoinduced CMRP. This catalytic system achieves the highly efficient and well-controlled polymerization of both less activated vinyl ester and more activated methacrylate. More remarkably, this catalytic system can facilely produce the di-/tri-block and even homogeneous random copolymers of vinyl ester and methacrylate. The mechanism studies are highly consistent with the polymerization results, which validate CMRP mechanism and our catalyst design concept. This work makes a breakthrough for efficiently accessing challenging copolymers of monomers with a very large difference in reactivity by rational catalyst design, which would contribute to the development of high-performance catalysts and polymer materials.

Methods

Materials

Unless stated otherwise, all manipulations with air- and moisture-sensitive chemicals and reagents were performed using standard Schlenk techniques on a dual-manifold line, or in an inert gas (Ar)-filled glovebox. Unless otherwise stated, the monomers vinyl acetate (VAc) (>99.0%, Tokyo Chemical Industry (TCI), Japan), vinyl butyrate (VBu) (>98.0%, TCI), vinyl pivalate (VPi) (>99.0%, Shanghai Acmec Biochemical Co., Ltd), methyl methacrylate (MMA) (>99.8%, TCI), and 2-methoxyethyl methacrylate (MEMA) (>95%, TCI) were purchased and dried over activated CaH_2 overnight, followed by vacuum distillation. Diphenyl(2,4,6-trimethylbenzoyl)phosphine oxide (TPO) (>97%, Beijing Innochem Science & Technology (Innochem)), cobalt(II) bromide (>99%, Beijing Hwrkchemical) and extra dry tetrahydrofuran (THF) (J&K) were used as received. Prior to characterization and

measurement, all polymers underwent comprehensive purification via quenching, adsorption, and filtration to ensure complete removal of cobalt complexes, unless otherwise specified.

Instruments and characterizations

Nuclear magnetic resonance (NMR) spectra were recorded on an Agilent 400 MHz spectrometer, or a Bruker 400 MHz spectrometer in chloroform-*d* at 298 K. Molecular weights were measured by the GPC equipped with a DAWN EOS multi-angle laser light scattering (MALLS with 18 angles) detector (Wyatt Technology) and a T-rEX refractive index detector (Wyatt S6 Technology) connected with three 300 × 8.0 mm columns of MZ-Gel SDplus 10E3Å 3 μm, 4 μm and 5 μm. The instrument was performed at 40 °C using THF eluent at a flow rate of 1 mL/min and calibrated using PMMA standards to give the relative molecular weight. High resolution mass spectra were determined on JMS-T100LP AccuTOF™ LC-Express (ESI) mass spectrometers. TGA was carried out on a TGA Q500 system. The instrument was equilibrated at 40 °C. The sample was heated up to 600 °C at a heating rate of 10 °C/min under nitrogen atmosphere. DSC was carried out on a DSC2A-013118, DSC2A-00307 and DSC Q2000 system. The sample was heated from 40 to 150 °C at a heating rate of 10 °C/min under nitrogen atmosphere, followed by cooling to −50 °C at 10 °C/min for two cycles. The reported DSC data was collected on the second heating cycle. Matrix-assisted laser desorption/ionization time-of-flight mass spectrometry (MALDI-TOF MS) was performed on a Bruker UltrafleXtreme TOF/TOF mass spectrometer (Bruker Daltonics GmbH & Co. KG, Bremen, Germany Bruker Daltonics, Inc., Billerica, MA) equipped with an Nd: YAG laser (355 nm). Trans-2-[3-(4-tert-butylphenyl)−2-methyl-2-propenyli-dene] malononitrile (DCTB, purchased from TCI) was applied as the matrix, and PMMA (M_n = 5.0 kDa) were used for calibration. The matrix was dissolved in $CHCl_3$ at 10 mg/mL, and the polymers were dissolved in $CHCl_3$ at 1 mg/mL. The sample was conducted in reflection mode. And the data analysis was conducted with Bruker's FlexAnalysis software. Sample preparation involved depositing 0.5 μL of matrix/salt mixture on the wells of a 384-well ground-steel plate, allowing the spots to dry, depositing 0.5 μL of each sample on top of a dry matrix/salt spot, and adding another 0.5 μL of matrix/salt on top of the dry sample (sandwich method); compared to the commonly used dry droplet method, in which a mixture of matrix/salt and sample is deposited onto the target plate, the sandwich method minimizes the disintegration of labile substances and allows for facile variation of the matrix to maximize the signal intensity. Elemental analysis of Br was acquired on 905 Titrando (Metrohm). The sample was fully combusted into the oxygen flask, according to the oxygen flask combustion method of *Pharmacopoeia of the People's Republic of China*. After the combustion products were completely absorbed into KOH aqueous solution (5 wt.%), the content of bromine in the aqueous solution was determined by potentiometric titration, according to *Chemical reagent - General rule for potentiometric titration (GB T 9725-2007)*.

Procedure for polymerization

General procedure for the synthesis of homopolymers. In a typical run, catalyst was made by mixing ligand and $CoBr_2$ ($[CoBr_2]_0$/$[ligand]_0$ = 1/1) in THF solution, which was stirred for 2 h. To the catalyst solution in a Pyrex Schlenk flask (with 2.2 cm diameter), allotted amounts of VAc and TPO were added. The mixture was irradiated using a white light with an output optical power of 24 W and a wavelength of 350–900 nm (Wuhan GeAo Chem Technology Co., Ltd) under argon atmosphere at ambient temperature (25 °C ± 5 °C) with magnetic stirring. A powerful fan was used to remove the heat of polymerization from the flask. After stirring for the allotted period, the polymerization reaction was quenched with chloroform (0.5 mL). Conversion was determined by integration of the monomer vs. polymer resonances in the ^{1}H NMR spectrum of the polymerization system. After completion of the reaction, the contents of the ampules were dissolved in DCM. The adsorption-treated filtrate was added to an approximately 50-fold excess of rapidly stirred *n*-hexane. The precipitate that formed was filtered, washed with *n*-hexane and dried to constant weight in vacuum.

General procedure for the synthesis of block copolymers. In a typical run, catalyst was made by mixing ligand and $CoBr_2$ ($[CoBr_2]_0$/$[ligand]_0$ = 1/1) in THF solution, which was stirred for 2 h. To the catalyst solution in a Pyrex Schlenk flask (with 2.2 cm diameter), allotted amounts of VAc and TPO were added. The mixture was stirred and irradiated by 24 W white light. After the allotted period, a small aliquot was taken in an anhydrous and oxygen-free environment, quenched by adding deuterium chloroform and analyzed to give the monomer conversion and polymer molecular weight. After the nearly complete conversion of VAc, allotted amounts of MMA and THF were added into the system in situ. The mixture continued to be stirred and irradiated by 24 W white light for the allotted period. Conversion was determined by the ^{1}H NMR spectrum of the polymerization system. After completion of the reaction, the contents of the ampules were dissolved in DCM. The adsorption-treated filtrate was added to an approximately 50-fold excess of rapidly stirred *n*-hexane. The precipitate that formed was filtered, washed with *n*-hexane and dried to constant weight in vacuum.

General procedure for the synthesis of random copolymers. In a typical run, catalyst was made by mixing ligand and $CoBr_2$ ($[CoBr_2]_0$/$[ligand]_0$ = 1/1) in THF solution, which was stirred for 2 h. To the catalyst solution in a Pyrex Schlenk flask (with 2.2 cm diameter), allotted amounts of VAc, MMA and TPO were added. The mixture was irradiated using a white light with an output optical power of 24 W and a wavelength of 350-900 nm (Wuhan GeAo Chem Technology Co., Ltd) under argon atmosphere at ambient temperature (25 °C ± 5 °C) with magnetic stirring. A powerful fan was used to remove the heat of polymerization from the flask. After stirring for the allotted period, the polymerization reaction was quenched with chloroform (0.5 mL). Conversion was determined by integration of the monomer vs. polymer resonances in the ^{1}H NMR spectrum of the polymerization system. After completion of the reaction, the contents of the ampules were dissolved in DCM. The adsorption-treated filtrate was added to an approximately 50-fold excess of rapidly stirred *n*-hexane. The precipitate that formed was filtered, washed with *n*-hexane and dried to constant weight in vacuum.

Data availability

All supplementary information relating to methods, mechanistic studies, computational studies, characterizations are available in Supplementary Information. Crystallographic data for **L4**/$CoBr_2$ (CCDC 2306200) and **L5**/$CoBr_2$ (CCDC 2306214) can be obtained free of charge from the Cambridge crystallo-graphic Data Centre via www.ccdc.cam.ac.uk/data request/cif. The cartesian coordinates of the optimized structures in this study are available as source data. All data are available from the corresponding author upon request. Source data are provided with this paper.

References

1. Arzamendi, G. & Asua, J. M. Monomer addition policies for copolymer composition control in semicontinuous emulsion copolymerization. *J. Appl. Polym. Sci.* **38**, 2019–2036 (1989).
2. Arzamendi, G. & Asua, J. M. Copolymer composition control during the seeded emulsion copolymerization of vinyl acetate and methyl acrylate. *Makromol. Chem. Macromol. Symposia* **35–36**, 249–268 (1990).
3. van Doremaele, G. H. J., Schoonbrood, H. A. S., Kurja, J. & German, A. L. Copolymer composition control by means of semicontinuous emulsion copolymerization. *J. Appl. Polym. Sci.* **45**, 957–966 (1992).

4. van Dorssen, H. Editorial. *Polymer* **36**, 3 (1995).
5. Urretabizkaia, A., Leiza, J. R. & Asua, J. M. On-line terpolymer composition control in semicontinuous emulsion polymerization. *AIChE J.* **40**, 1850–1864 (1994).
6. Mayo, F. R., Walling, C., Lewis, F. M. & Hulse, W. F. Copolymerization. V.1 Some Copolymerizations of Vinyl Acetate. *J. Am. Chem. Soc.* **70**, 1523–1525 (1948).
7. Dossi, M., Liang, K., Hutchinson, R. A. & Moscatelli, D. Investigation of Free-Radical Copolymerization Propagation Kinetics of Vinyl Acetate and Methyl Methacrylate. *J. Phys. Chem. B* **114**, 4213–4222 (2010).
8. Santos, A. M., Févotte, G., Othman, N., Othman, S. & McKenna, T. F. On-line monitoring of methyl methacrylate–vinyl acetate emulsion copolymerization. *J. Appl. Polym. Sci.* **75**, 1667–1683 (2000).
9. Islam, M. S., Yeum, J. H. & Das, A. K. Synthesis of poly(vinyl acetate–methyl methacrylate) copolymer microspheres using suspension polymerization. *J. Colloid Interface Sci.* **368**, 400–405 (2012).
10. Wang, H., Kolodka, E. & Tande, B. M. Thermomechanical and Rheological Studies of Copolymers of Methyl Methacrylate with a Series of Linear Vinyl Esters. *Ind. Eng. Chem. Res.* **52**, 5111–5119 (2013).
11. Ouchi, M., Terashima, T. & Sawamoto, M. Transition Metal-Catalyzed Living Radical Polymerization: Toward Perfection in Catalysis and Precision Polymer Synthesis. *Chem. Rev.* **109**, 4963–5050 (2009).
12. di Lena, F. & Matyjaszewski, K. Transition metal catalysts for controlled radical polymerization. *Prog. Polym. Sci.* **35**, 959–1021 (2010).
13. Nicolas, J. et al. Nitroxide-mediated polymerization. *Prog. Polym. Sci.* **38**, 63–235 (2013).
14. Hu, R., Leung, N. L. C. & Tang, B. Z. AIE macromolecules: syntheses, structures and functionalities. *Chem. Soc. Rev.* **43**, 4494–4562 (2014).
15. Li, B., Yu, B., Ye, Q. & Zhou, F. Tapping the potential of polymer brushes through synthesis. *Acc. Chem. Res* **48**, 229–237 (2015).
16. Hawker, C. J., Bosman, A. W. & Harth, E. New Polymer Synthesis by Nitroxide Mediated Living Radical Polymerizations. *Chem. Rev.* **101**, 3661–3688 (2001).
17. Benaglia, M. et al. Universal (Switchable) RAFT Agents. *J. Am. Chem. Soc.* **131**, 6914–6915 (2009).
18. Keddie, D. J. A guide to the synthesis of block copolymers using reversible-addition fragmentation chain transfer (RAFT) polymerization. *Chem. Soc. Rev.* **43**, 496–505 (2014).
19. Lin, Y.-C., Hsieh, Y.-L., Lin, Y.-D. & Peng, C.-H. Cobalt Bipyridine Bisphenolate Complex in Controlled/Living Radical Polymerization of Vinyl Monomers. *Macromolecules* **47**, 7362–7369 (2014).
20. Matyjaszewski, K. & Xia, J. Atom Transfer Radical Polymerization. *Chem. Rev.* **101**, 2921–2990 (2001).
21. Dworakowska, S., Lorandi, F., Gorczyński, A. & Matyjaszewski, K. Toward Green Atom Transfer Radical Polymerization: Current Status and Future Challenges. *Adv. Sci. (Weinh., Baden.-Wurtt., Ger.)* **9**, e2106076 (2022).
22. Iovu, M. C. & Matyjaszewski, K. Controlled/Living Radical Polymerization of Vinyl Acetate by Degenerative Transfer with Alkyl Iodides. *Macromolecules* **36**, 9346–9354 (2003).
23. Wayland, B. B., Poszmik, G., Mukerjee, S. L. & Fryd, M. Living Radical Polymerization of Acrylates by Organocobalt Porphyrin Complexes. *J. Am. Chem. Soc.* **116**, 7943–7944 (1994).
24. Kaneyoshi, H. & Matyjaszewski, K. Effect of Ligand and n-Butyl Acrylate on Cobalt-Mediated Radical Polymerization of Vinyl Acetate. *Macromolecules* **38**, 8163–8169 (2005).
25. Debuigne, A., Poli, R., Jérôme, C., Jérôme, R. & Detrembleur, C. Overview of cobalt-mediated radical polymerization: Roots, state of the art and future prospects. *Prog. Polym. Sci.* **34**, 211–239 (2009).
26. Peng, C.-H., Yang, T.-Y., Zhao, Y. & Fu, X. Reversible deactivation radical polymerization mediated by cobalt complexes: recent progress and perspectives. *Org. Biomolecular Chem.* **12**, 8580–8587 (2014).
27. Miao, X. et al. Photo-induced cobalt-mediated radical polymerization of vinyl acetate. *Polym. Chem.* **5**, 551–557 (2014).
28. Wang, Y. et al. A One-Step Route to CO2-Based Block Copolymers by Simultaneous ROCOP of CO2/Epoxides and RAFT Polymerization of Vinyl Monomers. *Angew. Chem. Int. Ed.* **57**, 3593–3597 (2018).
29. Demarteau, J., Debuigne, A. & Detrembleur, C. Organocobalt Complexes as Sources of Carbon-Centered Radicals for Organic and Polymer Chemistries. *Chem. Rev.* **119**, 6906–6955 (2019).
30. Nicolaÿ R., Kwak Y. & Matyjaszewski K. Synthesis of poly(vinyl acetate) block copolymers by successive RAFT and ATRP with a bromoxanthate iniferter. *Chem. Commun.* 5336–5338 https://doi.org/10.1039/B810778E (2008).
31. Tong, Y.-Y., Dong, Y.-Q., Du, F.-S. & Li, Z.-C. Synthesis of Well-Defined Poly(vinyl acetate)-b-Polystyrene by Combination of ATRP and RAFT Polymerization. *Macromolecules* **41**, 7339–7346 (2008).
32. Debuigne, A., Caille, J.-R., Willet, N. & Jérôme, R. Synthesis of Poly(vinyl acetate) and Poly(vinyl alcohol) Containing Block Copolymers by Combination of Cobalt-Mediated Radical Polymerization and ATRP. *Macromolecules* **38**, 9488–9496 (2005).
33. Kermagoret, A. et al. Expanding the Scope of Controlled Radical Polymerization via Cobalt–Tellurium Radical Exchange Reaction. *ACS Macro Lett.* **3**, 114–118 (2014).
34. Chen, Y.-J. et al. Hybridization of CMRP and ATRP: A Direct Living Chain Extension from Poly(vinyl acetate) to Poly(methyl methacrylate) and Polystyrene. *Macromolecules* **48**, 6832–6838 (2015).
35. Keddie, D. J., Moad, G., Rizzardo, E. & Thang, S. H. RAFT Agent Design and Synthesis. *Macromolecules* **45**, 5321–5342 (2012).
36. Ma, P. et al. Exhaustive Baeyer–Villiger oxidation: a tailor-made post-polymerization modification to access challenging poly(vinyl acetate) copolymers. *Chem. Sci.* **13**, 11746–11754 (2022).
37. Li, Y. et al. Ligand-Controlled Cobalt-Catalyzed Regiodivergent Alkyne Hydroalkylation. *J. Am. Chem. Soc.* **144**, 13961–13972 (2022).
38. Jiang, C. et al. Enantioselective Copper-Catalyzed Trifluoromethylation of Benzylic Radicals via Ring Opening of Cyclopropanols. *Chem* **6**, 2407–2419 (2020).
39. Baisch, U. & Poli, R. Copper(I/II) and cobalt(II) coordination chemistry of relevance to controlled radical polymerization processes. *Polyhedron* **27**, 2175–2185 (2008).
40. Debuigne, A. et al. Cobalt-mediated radical polymerization of acrylonitrile: kinetics investigations and DFT calculations. *Chem. (Weinh. der Bergstr., Ger.)* **14**, 7623–7637 (2008).
41. Chen Z.-H. et al Highly Efficient Atom Transfer Radical Polymerization System Based on the SaBOX/Copper Catalyst. **52**, 9792–9798 (2019).
42. Chen, Z.-H. et al. Winning Strategy for Iron-Based ATRP Using In Situ Generated Iodine as a Regulator. *ACS Catal.* **10**, 14127–14134 (2020).
43. Wang, X.-Y., Sun, X.-L., Wang, F. & Tang, Y. SaBOX/Copper Catalysts for Highly Syndio-Specific Atom Transfer Radical Polymerization of Methyl Methacrylate. *ACS Catal.* **7**, 4692–4696 (2017).
44. Li, Y.-N. et al. Hydrogen Bond Effects: A Strategy for Improving Controllability in Organocatalytic Photoinduced Controlled Radical Polymerization Targeting High Molecular Weight. *ACS Catal.* **12**, 11606–11614 (2022).
45. Wang, X.-Y., Chen, Z.-H., Sun, X.-L. & Tang, Y. Low temperature effect on ATRP of styrene and substituted styrenes enabled by SaBOX ligand. *Polymer* **178**, 121630 (2019).
46. Ma, Y. et al. Highly branched polymethacrylates prepared efficiently: brancher-directed topology and application performance. *Polym. Chem.* **12**, 6606–6615 (2021).

47. Ma, Y. et al. SaBOX/Copper-Catalyzed Synthesis, Degradation, and Upcycling of a PMMA-Based Copolymer. *Macromolecules* **56**, 7032–7042 (2023).
48. Hsu, C.-S., Yang, T.-Y. & Peng, C.-H. Vinyl acetate living radical polymerization mediated by cobalt porphyrins: kinetic–mechanistic studies. *Polym. Chem.* **5**, 3867–3875 (2014).
49. Debuigne, A., Caille, J.-R. & Jérôme, R. Highly Efficient Cobalt-Mediated Radical Polymerization of Vinyl Acetate. *Angew. Chem. Int. Ed.* **44**, 1101–1104 (2005).
50. Santhosh Kumar, K. S. et al. Electronic and steric ligand effects in the radical polymerization of vinyl acetate mediated by beta-ketoiminate complexes of cobalt(II). *Chem., Asian J.* **4**, 1257–1265 (2009).
51. Liao, C.-M., Hsu, C.-C., Wang, F.-S., Wayland, B. B. & Peng, C.-H. Living radical polymerization of vinyl acetate and methyl acrylate mediated by Co(Salen*) complexes. *Polym. Chem.* **4**, 3098–3104 (2013).
52. Zhao, Y. et al. A well-defined, versatile photoinitiator (salen) Co–CO2CH3 for visible light-initiated living/controlled radical polymerization. *Chem. Sci.* **6**, 2979–2988 (2015).
53. Murakami, M. Cover Picture: Achievements of the Late Professor Teruaki Mukaiyama (Chem. Rec. 1/2021). *Chem. Rec.* **21**, 1–1 (2021).
54. Zhao, Y., Yu, M. & Fu, X. Photo-cleavage of the cobalt–carbon bond: visible light-induced living radical polymerization mediated by organo-cobalt porphyrins. *Chem. Commun.* **49**, 5186–5188 (2013).
55. Kapil, K., et al. Visible-Light-Mediated Controlled Radical Branching Polymerization in Water. *Angew. Chem. (Int. ed. Engl.)* **62**, e202217658 (2023).
56. Xu, J., Jung, K., Atme, A., Shanmugam, S. & Boyer, C. A Robust and Versatile Photoinduced Living Polymerization of Conjugated and Unconjugated Monomers and Its Oxygen Tolerance. *J. Am. Chem. Soc.* **136**, 5508–5519 (2014).
57. Xu, J., Jung, K., Corrigan, N. A. & Boyer, C. Aqueous photoinduced living/controlled polymerization: tailoring for bioconjugation. *Chem. Sci.* **5**, 3568–3575 (2014).
58. Town, J. S., Jones, G. R. & Haddleton, D. M. MALDI-LID-ToF/ToF analysis of statistical and diblock polyacrylate copolymers. *Polym. Chem.* **9**, 4631–4641 (2018).
59. Pasch, H. & Schrepp, W. MALDI-TOF *Mass Spectrometry of Synthetic Polymers*. (2007).
60. Liu, S., Elyashiv, S. & Sen, A. Copper-mediated controlled copolymerization of methyl acrylate with 1-alkenes under mild conditions. *J. Am. Chem. Soc.* **123**, 12738–12739 (2001).
61. Kapil, K. et al. Hydrophilic Poly(meth)acrylates by Controlled Radical Branching Polymerization: Hyperbranching and Fragmentation. *Macromolecules* **57**, 5368–5379 (2024).
62. Lu, Y. & Yamago, S. One-Step Synthesis of Dendritic Highly Branched Polystyrenes by Organotellurium-Mediated Copolymerization of Styrene and a Dienyl Telluride Monomer. *Angew. Chem. Int. Ed.* **58**, 3952–3956 (2019).
63. Brandrup, J. et al. *Polymer Handbook*. (1999).
64. Hutchinson, R. A. & Penlidis, A. Free-Radical Polymerization: Homogeneous Systems. *In: Polymer Reaction Engineering*, (2007).
65. Lowry, G. G. The effect of depropagation on copolymer composition. I. General theory for one depropagating monomer. *J. Polym. Sci.* **42**, 463–477 (1960).
66. Mohammed, A. H., Ahmad, M. B., Ibrahim, N. A. & Zainuddin, N. J. P. Synthesis and monomer reactivity ratios of acrylamide with 3-(trimethoxysilyl)propyl methacrylate and tris(methoxyethoxy)vinylsilane copolymers. *Polimery* **61**, 758–765 (2016).
67. Muringayil Joseph, T., Murali Nair, S., Kattimuttathu Ittara, S., Haponiuk, J. T. & Thomas, S. Copolymerization of Styrene and Pentadecylphenylmethacrylate (PDPMA): Synthesis, Characterization, Thermomechanical and Adhesion Properties. *Polymers* **12**, 97 (2020).
68. Lundberg, D. J. et al. Accurate Determination of Reactivity Ratios for Copolymerization Reactions with Reversible Propagation Mechanisms. *Macromolecules* **57**, 6727–6740 (2024).
69. Ma, Y. D., Won, Y. C., Kubo, K. & Fukuda, T. Propagation and termination processes in the free-radical copolymerization of methyl methacrylate and vinyl acetate. *Macromolecules* **26**, 6766–6770 (1993).
70. Autzen, A. A. A. et al. IUPAC recommended experimental methods and data evaluation procedures for the determination of radical copolymerization reactivity ratios from composition data. *Polym. Chem.* **15**, 1851–1861 (2024).

Acknowledgements

The authors are grateful for financial support by the National Natural Science Foundation of China (22271304, X.-Y.W.), Science and Technology Commission of Shanghai Municipality (23ZR1476300, 23JC1404500, X.-Y.W.) and the Strategic Priority Research Program of the Chinese Academy of Sciences (XDB1180000, X.-Y.W.).

Author contributions

X.-Y.W. and Y.T. conceived the study and planned the research; Y.-J. D., Y.-N.L., S.-Y.Y., K.H. and J.-F.L. synthesized and characterized the compounds and polymers; S.-Y.Z. and Y.Z. conducted the DFT calculations and analysis; X.-Y.W. and Y.T. prepared the manuscript; all the authors commented on the manuscript.

Competing interests

The authors declare no competing interests.

Additional information

Supplementary information The online version contains supplementary material available at https://doi.org/10.1038/s41467-025-62145-7.

Correspondence and requests for materials should be addressed to Xiao-Yan Wang or Yong Tang.

Peer review information *Nature Communications* thanks the anonymous reviewers for their contribution to the peer review of this work. A peer review file is available.